Surface-Enhanced Infrared Absorption Spectroscopic Chalcogenide Waveguide Sensor Using a Silver Island Film

Mingquan Pi, Chuantao Zheng,* Jialin Ji, Huan Zhao, Zihang Peng, Jiaming Lang, Lei Liang, Yu Zhang, Yiding Wang, and Frank K. Tittel
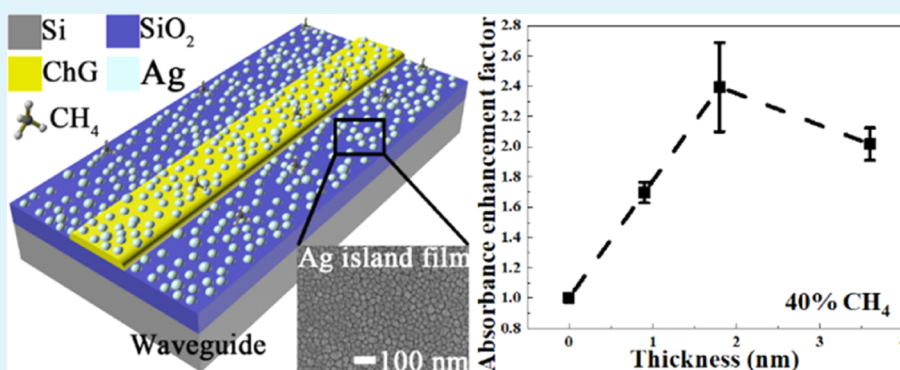
ACCESS | Metrics & More | Article Recommendations | Supporting Information

ABSTRACT: A surface-enhanced infrared absorption spectroscopic chalcogenide waveguide sensor based on the silver island film was proposed for the first time to enhance the sensing performance in both liquid and gas phases. The chalcogenide waveguide sensor was fabricated by the lift-off and oblique angle deposition methods. The surface morphology of the silver island film with different thicknesses was characterized. The absorption of ethanol (liquid) at a wavelength of 1654 nm and that of methane (gas) at 3291 nm were measured using the fabricated chalcogenide waveguide sensor. The chalcogenide waveguide sensor integrated with the 1.8 nm-thick silver island film revealed the best sensing performance. With an acceptable increased waveguide loss resulting from the fabrication of the film, the absorbance enhancement factors for ethanol and methane were experimentally obtained to be >1.5 and >2.3, respectively. The 1σ limit of detection of methane for the sensor integrated with the 1.8 nm-thick silver island film was ∼4.11% for an averaging time of 0.2 s. The mathematic relation between the absorbance enhancement factor and the waveguide loss was derived for sensing performance improvement. Also, the proposed rectangular waveguide sensor provides an idea for the design of a sensor-on-a-chip instead of other waveguide sensors with a high requirement of fabrication accuracy, for example, a slot waveguide or a photonic crystal waveguide.

KEYWORDS: surface-enhanced infrared absorption spectroscopy, chalcogenide waveguide, waveguide sensor, silver island film, gas detection, liquid detection

1. INTRODUCTION

Infrared absorption spectroscopy has been maturely applied to the analysis and characterization of gas and liquid analytes.[1−5] However, a sensor system consisting of discrete components and modules usually has a large size and heavy weight, which is not preferred for portable sensing applications. At the same time, environmental vibrations and high power consumption also limit the application of such sensors. On the contrary, an on-chip optical waveguide sensor based on the evanescent field can overcome these problems by integrating a laser, a sensing waveguide, and a detector on a single chip.[6] However, the small light−matter interaction waveguide length, the large waveguide loss, and the small filling factor limit the performance of a waveguide sensor.[7,8]

On one hand, both the waveguide material and the structure affect the performance of a waveguide sensor.[9−11] Generally, the absorption line strength of an analyte in the near-infrared (NIR) range is at least 2 orders smaller than that in the mid-infrared (MIR) region. Therefore, using a waveguide sensor with a low absorption loss in the MIR range can improve the gas-sensing performance. As we know, silica (SiO_2) has a high optical loss in the MIR range (>3.6 μm), which does not allow
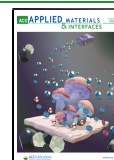
the silicon-on-insulator (SOI) waveguide for MIR applications. As an alternative to the SOI waveguide, chalcogenide (ChG) glass with a high refractive index (>2.0) is transparent from the NIR region to the MIR region,[12] which can serve as a good candidate for MIR measurement.

On another hand, the cross-sectional structure determines the filling factor of a waveguide,[13,14] which shows that the evanescent mode field accounts for the proportion of all light. A vertical slot waveguide can confine the light in the slot area to enlarge the filling factor. However, the fabrication process of a slot waveguide is complicated, and the sidewall of the slot fabricated by dry etching is usually rough, which increases the scattering loss and decreases the sensing performance.[15] Previously, our group proposed a suspended slot waveguide[16] and a horizontal slot waveguide[17] to increase the filling factor, but their fabrication process is also more complex than that of a rectangular waveguide. Different from the slot waveguide, a ChG rectangular waveguide can be easily fabricated by the lift-off method without etching to decrease the scattering loss. To minimize the device size, meander[18] and spiral waveguides[19] were proposed for light−matter interaction enhancement within a compact footprint size. Though a microring resonator can increase the effective interaction length, the resonant wavelength is difficult to be aligned with the gas absorption peak,[17] and the coupling distance with the submicron size is hard to be controlled without electron beam lithography (EBL).

Besides, in addition to increasing the waveguide length and filling factor, some physical effects can be utilized to improve the sensing performance. The slow light effect in a photonic crystal waveguide (PCW) or a subwavelength grating waveguide was utilized to improve the effective optical path length.[20−22] However, the propagation loss of such a waveguide is usually large,[23] and a PCW should be fabricated by EBL through a high-cost and long-time procedure. The adsorptive material can be coated on the waveguide as an upper cladding layer to increase the local concentration of the analyte, but the adsorption and desorption processes need a long response time.[24] Refractive index sensing is another commonly used waveguide-sensing method, but a refractive index sensor without an adsorptive cladding layer or a selective cladding layer has poor selectivity for analytes. In addition, for waveguide gas sensing, the relative wavelength change ($\Delta\lambda/\lambda$) based on refractive index sensing is less sensitive than the relative power change ($\Delta P/P$) based on optical absorption because the refractive index change of gas is low due to the concentration change.[17] In 2018, Chen et al. integrated Au nanorods on an SOI rib waveguide for surface-enhanced infrared absorption (SEIRA) spectroscopy for the first time.[25] The output laser beam intensity was improved because the analyte changed the coupling efficiency of light to the Au nano-antenna.[25−27] However, the absorption of an analyte cannot be directly decided according to the change in the output light intensity. The resonant peak influenced by the fabrication error will be difficult to align with the absorption peak, and the nano-antenna needs to be fabricated by EBL. Alternatively, the metal island film with a rough island nanostructure is designed to produce the SEIRA effect, which can be easily fabricated by the oblique angle deposition method.[28,29]

In this work, in order to obtain a waveguide sensor-on-a-chip with an improved sensing performance both in the NIR and MIR ranges, for the first time as we know, we propose an efficient method to increase the light−matter interaction by depositing a silver (Ag) island film on the surface of the ChG rectangular waveguide. The novel aspects of this sensor include the following: (1) the waveguide sensor with a Ag island film introduces the SEIRA effect to improve the sensing performance; (2) the lift-off method and oblique angle deposition method were used in the fabrication of the SEIRA spectroscopic waveguide sensor, which are simple and fast for sensor fabrication; (3) absolute ethanol (C_2H_6O), water (H_2O), and methane (CH_4) were used as liquid and gas analytes to verify the SEIRA effect; and (4) shale gas measurement was performed to show the normal operation of the on-chip waveguide sensing technique.

2. EXPERIMENTAL SECTION

2.1. Sensor Fabrication Process. The ChG waveguide sensor was fabricated on a silicon (Si) substrate with a 2 μm-thick oxide layer. The fabrication process diagram is shown in Figure 1. First, the
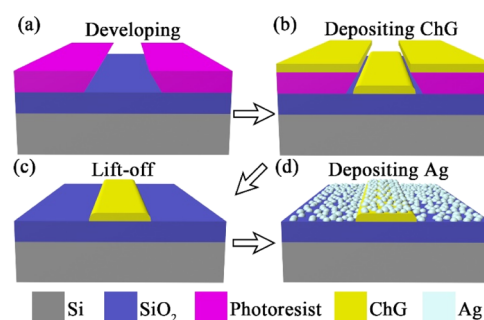

Figure 1. Fabrication process of the waveguide sensor based on a Ag island film. (a) Developing after the lithography to form the undercut structure. (b) Depositing the chalcogenide film. (c) Chalcogenide waveguide fabrication using the lift-off method. (d) Depositing the Ag island film.

RN-218 photoresist (Suzhou Research Semiconductor, China) was spun on the substrate. The undercut structure of the RN-218 photoresist with a thickness of ∼5.5 μm was fabricated by lithography and developing (Figure 1a). The exposure dose and development time were 60 mJ/cm^2 and 180 s, respectively. Then, a $Ge_{28}Sb_{12}Se_{60}$ film was deposited on the substrate by thermal evaporation (IT-302, LJUHV), and the evaporation rate was ∼1.2 nm/s (Figure 1b). In the next step, the ChG waveguide was fabricated by the lift-off method (Figure 1c). Finally, an Ag island film was deposited on the ChG waveguide by thermal evaporation (Figure 1d) with an evaporation rate of ∼0.1 nm/s, and the film thickness was determined by a surface profiler (Dektak 150, Veeco). The oblique angle of the substrate was set to be 45°. This was realized by fixing a 3D-printed sample table with an oblique angle of 30° with the umbrella frame, which has an oblique angle of 15°.

2.2. Waveguide Sensor Structure. The optical waveguide sensor includes a coupling area and a sensing area. To improve the coupling efficiency between the waveguide and the fiber, the waveguide width in the coupling area is 16 μm and the length of the taper transition waveguide is 300 μm. Both the straight waveguide with a length of 1 cm and the meander waveguide with a length of 2 cm were fabricated on the same substrate. The bending radius of the meander waveguide was increased to 50 μm to decrease the bending loss. The top-view structure of the waveguide sensor is shown in Figure 2b, and the local scanning electron microscopy (SEM) images of the two sensing waveguides are shown in Figure 2a,c, respectively. The straight waveguide and meander waveguide were used for the successive liquid and gas sensing, respectively. The SEM image of the waveguide cross-sectional structure in the sensing area without the Ag island film is shown in Figure 2d. The width and height of the waveguide core layer are 6 and 0.3 μm, respectively. The COMSOL
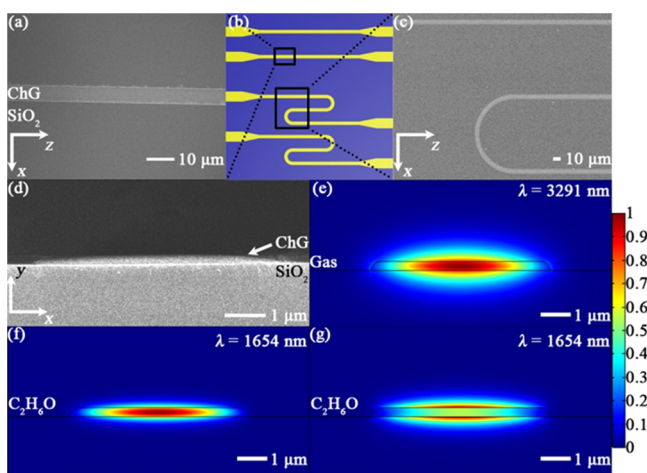
Figure 2. (a) Zoomed SEM image of the straight waveguide sensing area. (b) Structural diagram of the straight waveguide sensor and the meander waveguide sensor. (c) Zoomed SEM image of the meander waveguide sensing area. (d) SEM image of the waveguide cross-sectional structure without the Ag island film. (e) Quasi-TE$_0$ mode field distribution of the chalcogenide waveguide with a CH$_4$ upper cladding layer at 3291 nm. (f) Quasi-TE$_0$ mode and (g) quasi-TM$_0$ mode field distribution of the chalcogenide waveguide with an C$_2$H$_6$O upper cladding layer at a wavelength of 1654 nm.

Multiphysics software was used to simulate the optical mode field distribution. The refractive indices of Ge$_{28}$Sb$_{12}$Se$_{60}$ and SiO$_2$ are ~2.6 and ~1.4, respectively. As a kind of liquid analyte, the refractive index of C$_2$H$_6$O is 1.35 at 1654 nm, and the refractive index of CH$_4$ is ~1. The extinction coefficient κ of C$_2$H$_6$O versus wavelength is shown in Figure 4c, and the κ at 1654 nm is ~4.7 × 10^{-5}.[30] At 1654 nm, the quasi-TE$_0$ mode and quasi-TM$_0$ mode field distributions of the ChG waveguide with an C$_2$H$_6$O upper cladding layer are shown in Figure 2f,g, respectively. As a flammable and explosive gas, CH$_4$ was used as the gas analyte. The absorption spectrum of 50 parts-per-million (ppm) CH$_4$ near 3291 nm is shown in Figure 4d based on the HITRAN database, where the temperature is 298 K, the pressure is 1 atm, and the optical path length is 10 cm. The absorbance of pure CH$_4$ is 10.715 cm^{-1}.[16] Simulation results show that the waveguide only guided the quasi-TE mode light at a wavelength of 3291 nm, and the quasi-TE$_0$ mode field distribution is shown in Figure 2e.

2.3. Ag Island Film Morphology. The SEM images of the Ag island film with thicknesses of 0.9, 1.8, 3.6, and 5.4 nm on the SiO$_2$ layer are shown in Figure 3a−d, respectively. As can be seen, the size of the Ag island becomes larger with the increase in the film thickness, and there is no obvious island structure when the thickness of the Ag
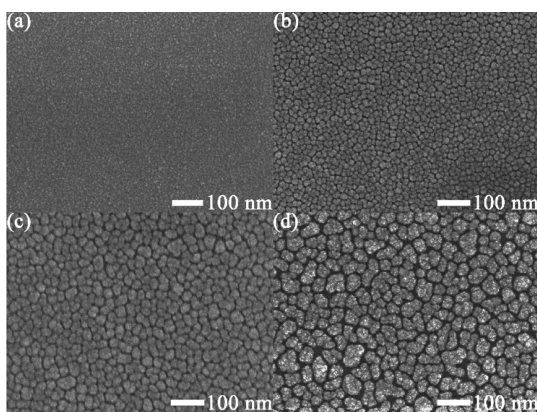
island film is only 0.9 nm. Five ChG waveguide samples were fabricated, named as WG1, WG2, WG3, WG4, and WG5, with the Ag island film thicknesses of 0, 0.9, 1.8, 3.6, and 5.4 nm, respectively. Except for the film thickness, other structural parameters of the five sensors are totally the same. The SEM images of all the sensor samples including the straight waveguide and meander waveguide using the Ag island film with different thicknesses are shown in Figure S1.

2.4. Waveguide Sensor System. The diagram of the NIR waveguide liquid sensor system and the diagram of the MIR waveguide gas sensor system are shown in Figure 4a,b, respectively. For the NIR waveguide liquid sensor system, a distributed feedback (DFB) laser (Sichuan Tengzhong light technology, China) emitting at a central wavelength of ~1654 nm was used as the laser source for C$_2$H$_6$O measurement. A current driver (LDC210C, Thorlabs) and a temperature controller (TED200C, Thorlabs) were used to control the current and temperature of the laser, respectively. The laser beam was coupled to a straight waveguide through a single-mode (SM) lensed fiber, and the light output from the waveguide was collected by a multimode (MM) fiber. A germanium (Ge) detector (PDA50B2, Thorlabs) was used to convert the light output from the fiber collimator to an electrical signal. For the MIR waveguide gas sensor system, an interband cascade laser (ICL, Nanoplus) emitting at a central wavelength of ~3291 nm was used as the light source for CH$_4$ measurement, which was driven by a current driver (LDC210C, Thorlabs) and a temperature controller (TED200C, Thorlabs). The light from the laser was coupled to a fluoride fiber by a reflective lens (RC08, Thorlabs) and butt-coupled to the meander waveguide. A mercury cadmium telluride detector (PVI-4TE-5, VIGO System) was used to measure the signal output from the waveguide. For the two sensing systems, a microscope was used to observe the positions of the fiber and the waveguide for alignment. The electrical signals from the two detectors were obtained by a data acquisition (DAQ) card (USB6361, National Instruments), and a LabVIEW platform was used to control the laser current and process the two electrical signals.

3. RESULTS AND DISCUSSION

3.1. Experimental Results for Liquid Sensing. In the C$_2$H$_6$O sensing experiment, straight waveguides with a sensing length of 1 cm were used for measurement. The temperature and current of the DFB laser were set to be 16 °C and 60 mA, respectively, resulting in an output wavelength of ~1654 nm. The laser beam output from the ChG waveguide with air cladding was obtained by the detector and converted into an electrical signal, which can be treated as a background signal without absorption. Then, C$_2$H$_6$O was dropped on the straight waveguide, and the amplitude of the electrical signal was decreased, which obeys the Lambert−Beer law as[16]

$$V = V_0 \exp(-\gamma \alpha C L - \alpha_{\text{int}} L) \tag{1}$$

where V is the amplitude of the output electrical signal from the waveguide sensor with an analyte; V_0 is the corresponding input signal amplitude; α and α_{int} are the absorption coefficient of the analyte and the waveguide intrinsic loss, respectively; C and L are the analyte concentration and the sensing waveguide length, respectively; and γ is a filling factor which can be expressed as[31]

$$\gamma = \frac{n_g \iint_{\text{analyte}} \varepsilon(x, y)|E(x, y)|^2 \mathrm{d}x \, \mathrm{d}y}{\iint_{\text{total}} \varepsilon(x, y)|E(x, y)|^2 \mathrm{d}x \, \mathrm{d}y} \tag{2}$$

where n_g is the group refractive index; E is the electric field; and ε is the permittivity. The absorbance is defined as $-\ln(V/V_0)$, which indicates the strength of the absorption. Note that the loss of the SEIRA spectroscopic waveguide sensor based on a Ag island film mainly includes scattering loss resulting from
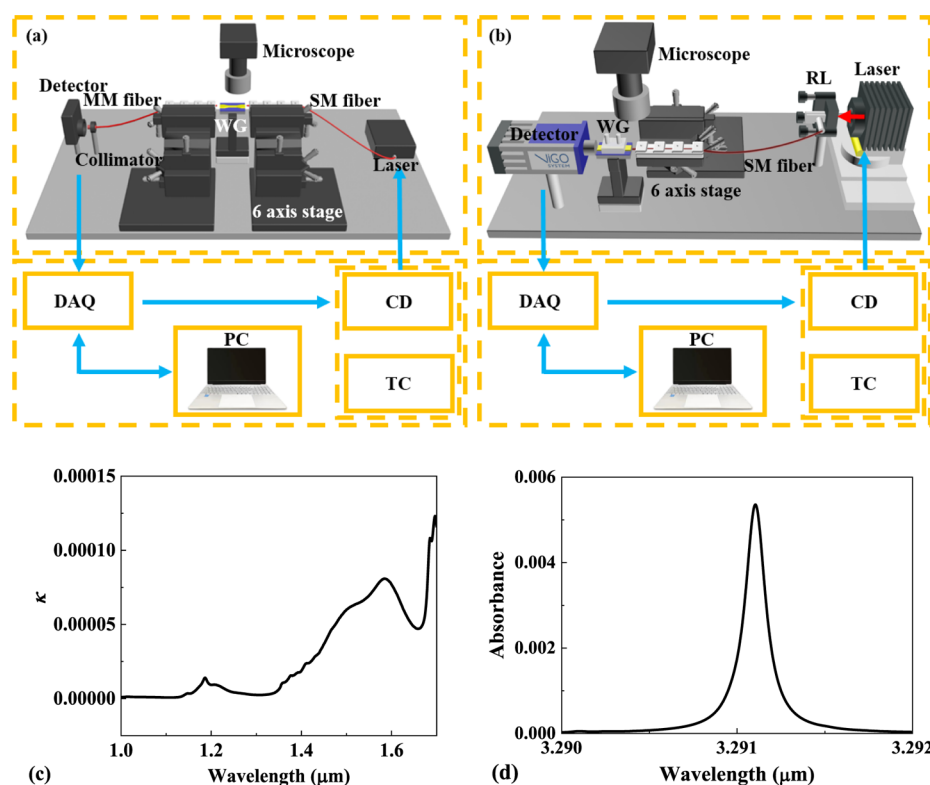

Figure 3. SEM images of the Ag island film on the SiO$_2$ layer with thicknesses of (a) 0.9 nm, (b) 1.8 nm, (c) 3.6 nm, and (d) 5.4 nm.

Figure 4. (a) NIR waveguide liquid sensor system. (b) MIR waveguide gas sensor system. WG: waveguide; CD: current driver; TC: temperature controller; RL: reflective lens; SM: single mode; MM: multimode; PC: personal computer; and DAQ: data acquisition. (c) Extinction coefficient of C_2H_6O vs wavelength. (d) Simulated 50 ppm CH_4 absorption spectrum near 3291 nm, where the temperature is 298 K, the pressure is 1 atm, and the optical path length is 10 cm.
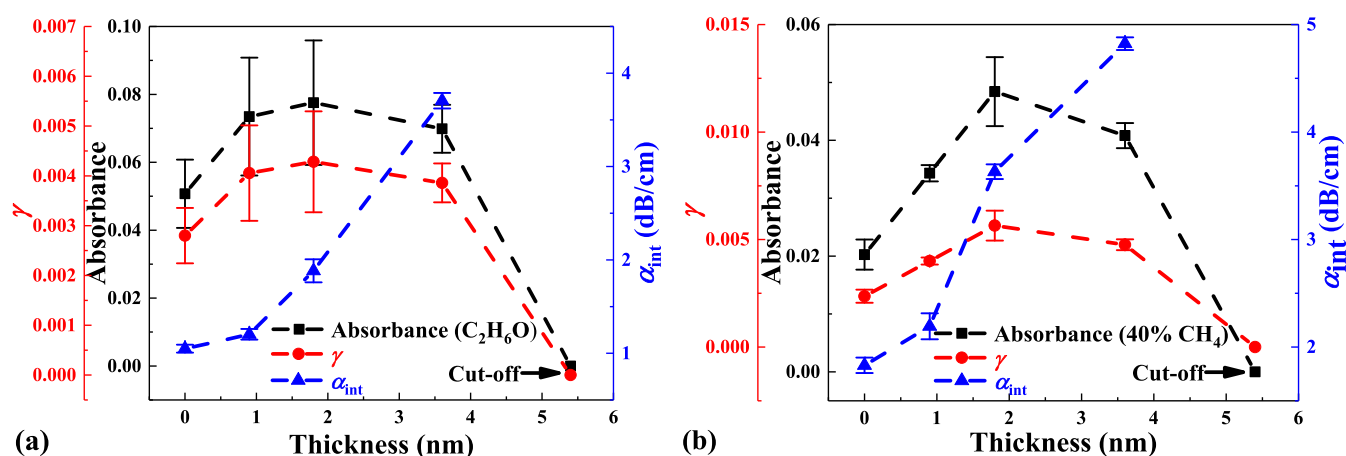

Figure 5. (a) Curves of the measured absorbance of C_2H_6O, filling factor, and waveguide intrinsic loss vs the thickness of the Ag island film. (b) Curves of the measured absorbance of 40% CH_4, filling factor, and waveguide intrinsic loss vs the thickness of the Ag island film.

the rough waveguide surface and the absorption loss from waveguide materials, which can be decreased by a thermal reflow process.[32]

Curves of the absorbance $[-\ln(V/V_0)]$ of C_2H_6O, γ, and α_{int} versus the thickness of the Ag island film are shown in Figure 5a, where α_{int} is obtained by the cutoff method and γ is obtained by eq 1. The absorbance enhancement factor (EF) is defined as the ratio between the absorbance of the sensor with a Ag island film divided by the absorbance of the sensor without the Ag island film, that is, $[-\ln(V/V_0)|_{island}]/[-\ln(V/V_0)|_{no\ island}]$. The main factors affecting the absorption performances of the waveguide sensor include local surface

optical field intensity and waveguide loss. The enhancement of the local surface optical field intensity is originated mainly from the surface plasmon resonance effect of the Ag island film.[28] When the Ag island film is too thin, the local field enhancement effect is weak, but the waveguide loss is low. The waveguide loss becomes larger and may not guide light when the thickness of the Ag island film increases to a certain value (e.g., 5 nm) because both the absorption loss and scattering loss are too large. That is why the WG5 sensor is cut off in mode propagation. The local field enhancement effect is also related to the thickness of the Ag island film. With the increase in the Ag island film thickness at first, the quantity of
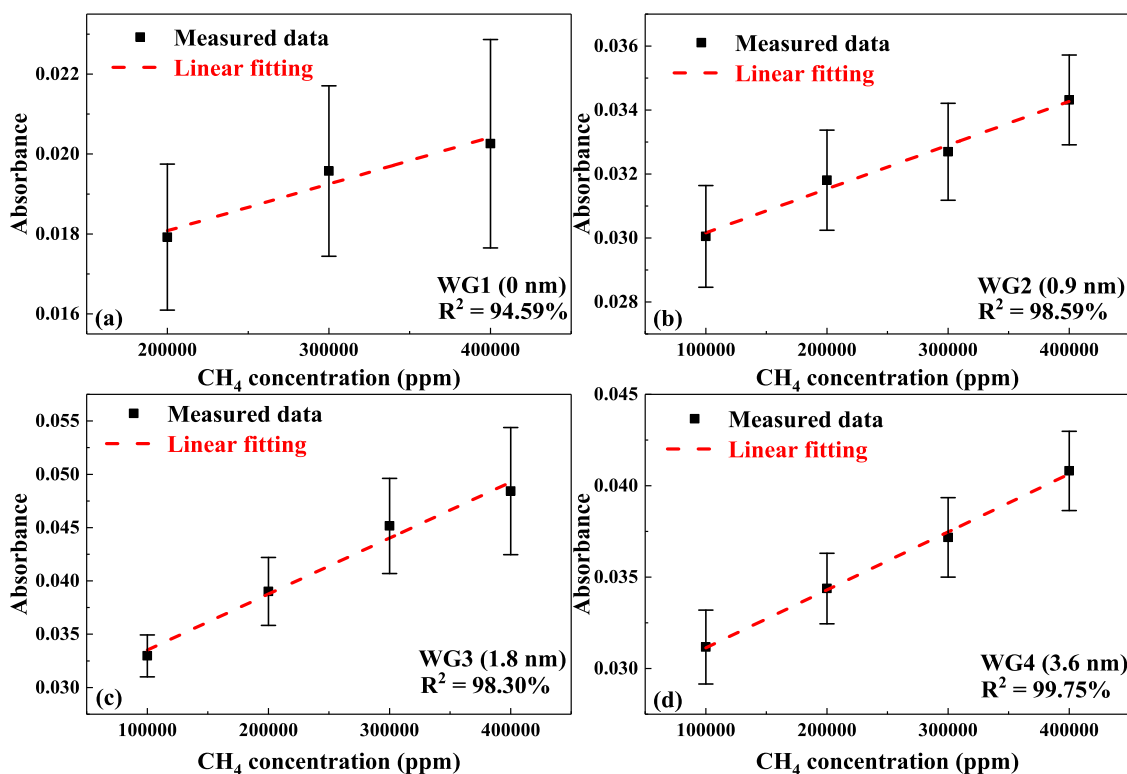
Figure 6. Absorbances of (a) WG1, (b) WG2, (c) WG3, and (d) WG4 at four CH_4 concentration levels of 10, 20, 30, and 40%. R^2: goodness of fit.

Ag islands gets larger, the distance between Ag islands gets smaller, the interaction effect becomes stronger between Ag islands, and the local field effect is strengthened too. However, as the thickness of the Ag island film continues increasing, the size of the Ag islands becomes larger and its quantity decreases, which weakens the local field enhancement effect. Thus, there is an optimum value of the thickness of the Ag island film at which we can achieve the maximum absorption enhancement. The experiment results show that the waveguide sensor with the 1.8 nm-thick Ag island film (WG3) has the highest EF (>1.5) and the increase in the waveguide loss is <1 dB/cm, which is acceptable for output light detection. Thus, WG3 shows the best performance among the five fabricated waveguide sensors. Similar phenomena can be found in related metal island film sensing experiments.[28,29,33,34]

Besides, experimental results of liquid water sensing at an absorption wavelength of 1368 nm can be found in the Supporting Information, which shows a similar sensing performance change trend (Figure S3b), and the maximum EF is >2.3 when the film thickness is 1.8 nm.

3.2. Experimental Results for Gas Sensing. Meander waveguides with a sensing length of 2 cm were used for CH_4 measurement based on the direct absorption spectroscopy (DAS) technique. A polydimethylsiloxane (PDMS) gas cell with an inlet and an outlet was bonded on the substrate. The temperature of the ICL was set to be 16 °C, and the scan current range was set to be 42−58 mA to cover the CH_4 absorption line at 3038.5 cm^{-1}. Nitrogen (N_2, 99.999%) was used to balance the CH_4 (99.999%) concentration by a gas-mixing system (Series 4000, Environics) to obtain the target CH_4 concentration.

Curves of the absorbance of 40% CH_4, γ, and α_{int} versus the thickness of the Ag island film are shown in Figure 5b. The WG5 sensor shows a cutoff region in mode propagation, and

the sensing performance change trend looks the same as that of C_2H_6O for a similar reason. The EF is >2.3 when the film thickness is 1.8 nm, and the increase in α_{int} for WG3 is <2 dB/cm.

As a conclusion, the experimental results of C_2H_6O, H_2O, and CH_4 show that the enhancement effect of the Ag island film can be used at different wavelengths from the NIR range to the MIR range.

The absorbances of WG1, WG2, WG3, and WG4 at four CH_4 concentration levels of 10, 20, 30, and 40% are shown in Figure 6a−d, respectively. WG1 without the enhancement effect is unable to detect CH_4 with a concentration level of 10% because of low absorbance. The linearity of the WG1 linear fitting curve is lower than those of WG2, WG3, and WG4. The linear fitting equations of the four sensors between CH_4 concentrations C_{WG1}, C_{WG2}, C_{WG3}, and C_{WG4} (in ppm) and the absorbance (Amp_{DAS}, in V) are

$$Amp_{DAS} = 1.16861 \times 10^{-8} C_{WG1} + 0.01575 \tag{3}$$

$$Amp_{DAS} = 1.36930 \times 10^{-8} C_{WG2} + 0.02879 \tag{4}$$

$$Amp_{DAS} = 5.24903 \times 10^{-8} C_{WG3} + 0.02827 \tag{5}$$

$$Amp_{DAS} = 3.17224 \times 10^{-8} C_{WG4} + 0.02795 \tag{6}$$

According to the experimental results, the limit of detection (LoD) can be calculated as[35]

$$LoD = C/SNR_C \tag{7}$$

where SNR_C is the signal-to-noise ratio under a concentration level of C. In the same sensing system, the theoretical noise level should be the same, but the environmental vibration and gas concentration variation also cause the change in the noise level. Here, the maximum error of the averaged absorbance for

the 40% CH_4 sample (8.96×10^{-4}) is considered as the system noise. Therefore, the LoDs of WG1, WG2, WG3, and WG4 were calculated to be 5.99, 3.54, 2.51, and 2.97%, respectively. WG3 with the 1.8 nm-thick Ag island film and the lowest LoD reveals the best performance among the fabricated five waveguide sensors, which is consistent with the measured absorbance curve shown in Figure 5b.

An Allan deviation analysis was performed by the measurement of the absorbance under a pure N_2 environment over a time period of 120 s. The Allan deviation plots of WG1, WG2, WG3, and WG4 versus the averaging time are shown in Figure 7. As can be seen, WG2, WG3, and WG4 reveal a lower LoD
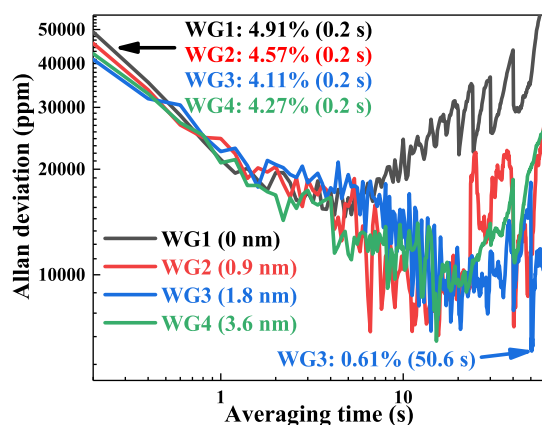

Figure 7. Allan deviation plots of WG1, WG2, WG3, and WG4 vs averaging time.

than that of WG1 due to the absorption enhancement of the Ag island film. As the averaging time increases, the three waveguide sensors with the Ag island film reveal better stability since the Allan deviation continues to decrease as the averaging time increases to 10 s. When the averaging time is 0.2 s, WG3 shows a 1σ LoD of 4.11% (σ is the Allan deviation), which is lower than those of WG2 and WG4. These results are consistent with the absorbance curve in Figure 5b. The 1σ

LoD of WG3 with the optimum averaging time of 50.6 s is 0.61%.

3.3. Application of the Waveguide Sensor for Shale Gas Measurement. An application of the waveguide sensor was performed for shale gas measurement, which is of great significance for the exploration of natural gas resources. The major component of shale gas is CH_4.[36] Shale gas samples obtained at the fracturing temperatures of 450, 550, and 650 °C were stored in three gas bags (Figure 8c) and were squeezed into the PDMS gas cell. The measured CH_4 concentration levels of the shale gas samples are shown in Figure 8a, and the absorbance curves by Lorentz fitting of the three samples are shown in Figure 8d−f, respectively. The CH_4 concentration levels at 550 °C (∼27%) is the highest in the three samples. The curve of observed CH_4 concentration levels of the shale gas samples obtained at a fracturing temperature of 550 °C versus observation time is shown in Figure 8b. A short response time of <0.2 s was obtained. The fluctuation of the measured CH_4 concentration levels of the shale gas sample is probably caused by the change of the gas flow when squeezing the gas bags, and both the environmental noise and system interference account for the variation. The measurement of shale gas shows that the SEIRA spectroscopic ChG waveguide sensor can be put into field applications, for example, the exploration of natural gas resources.

3.4. Requirement of the Waveguide Sensor for Absorption Enhancement. The purpose of fabricating a metal island film is to enhance the absorption (e.g., improve the sensitivity). However, the waveguide loss will increase due to the fabrication of the film, which will decay the sensing performance. Therefore, the effects of the enhanced absorption and the increased α_{int} on the performance of a sensor should be considered. Through theoretical derivation (see the Supporting Information), the LoD can be decreased after depositing the Ag island film when

$$E_\gamma > \frac{\text{LoD}(E_\gamma = 1, \qquad \alpha_{int} = \alpha_{int2})}{\text{LoD}(E_\gamma = 1, \qquad \alpha_{int} = \alpha_{int1})} \qquad (8)$$

where α_{int1} and α_{int2} are the intrinsic losses of the waveguide sensor without a Ag island film and the waveguide sensor
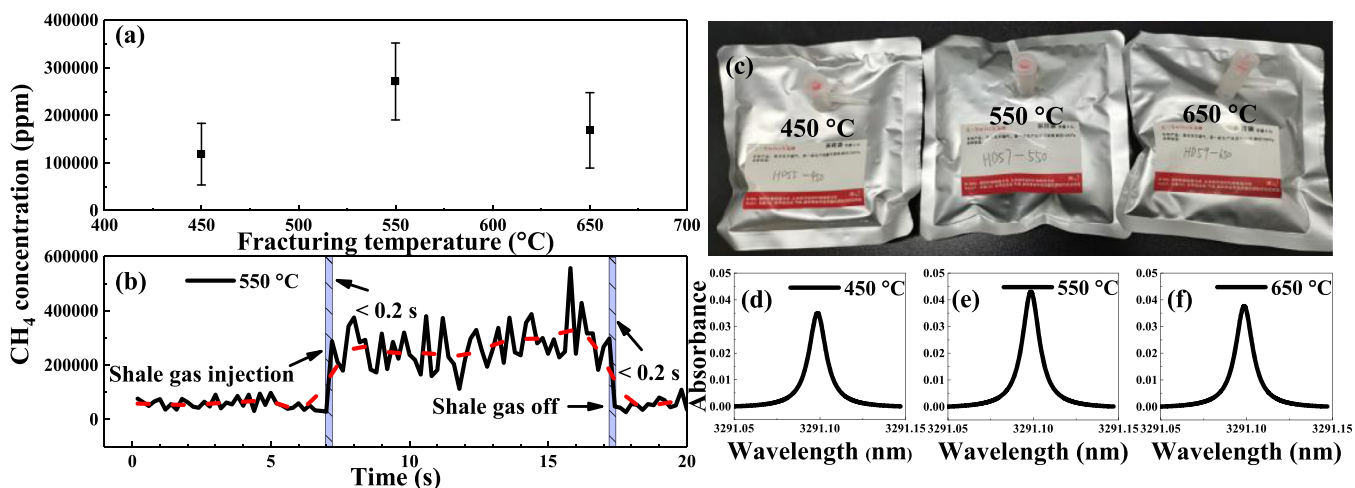

Figure 8. (a) Measured CH_4 concentration levels for the three shale gas samples obtained at the fracturing temperatures of 450, 550, and 650 °C. (b) Time response of CH_4 concentration detection by injecting the shale gas sample with a fracturing temperature of 550 °C into the PDMS gas cell. (c) Three shale gas samples in gas bags obtained at the fracturing temperatures of 450, 550, and 650 °C. Measured absorbance curves by Lorentz fitting of three shale gas samples at the fracturing temperatures of (d) 450 °C, (e) 550 °C, and (f) 650 °C.

integrated with a Ag island film, respectively. The enhancement of γ (denoted by E_γ) is defined as the γ of the sensor with a Ag island film divided by the γ of the sensor without a Ag island film. The right side of eq 8 represents the ratio between the two LoDs resulting from the increase of α_{int}.

3.5. Comparison and Discussion. A comparison between WG3 and other MIR ChG waveguide CH_4 sensors is shown in Table 1. As can be seen, the fabricated WG3 has lower α_{int} and

Table 1. Comparison between WG3 and Other MIR ChG Waveguide CH_4 Sensors

refs.	wavelength (μm)	technique	L (cm)	α_{int} (dB/cm)	response time (s)	LoD (%)
19	3.31	DAS	2	7		2.5
37	3.31	DAS	0.5	8		1
this work	3.291	DAS	2	3.6	<0.2	0.61

LoD values compared with that of other ChG waveguide CH_4 sensors. Decreasing the waveguide width and optimizing the thickness of the Ag island film can improve γ, which can lead to further improvement of the sensing performance. Because of a small waveguide loss, the waveguide length can be further increased to improve the absorbance. Other gas-sensing techniques (e.g., wavelength modulation spectroscopy) can be used to suppress the optical interference and to improve the signal-to-noise ratio.

A second comparison among the waveguide sensors based on optical absorption using different enhancement methods is shown in Table S1. The slot waveguide fabricated by dry etching tends to have a high propagation loss, which is a key problem for sensing.[15] Though PCW can achieve a high group index to increase γ, the structural parameters need to be strictly controlled in the fabrication process, otherwise the slow light wavelength will change, leading to the failure to improve the sensing performance. A microcavity waveguide (e.g., microrings and microdisks) can achieve a large effective optical path length, but the resonance wavelength is easily affected by fabrication errors.[17] Though the enhancement factor is smaller than that of other methods, the waveguide sensing technique based on a Ag island film has no need for high fabrication precision, and the absorption enhancement effect can be realized in both NIR and MIR ranges, which extends the application of such techniques to both liquid and gas detection.

A third comparison among three gas-sensing methods is shown in Table S2, including electrochemical, refractive index, and optical absorption methods. Some electronic gas sensors (e.g., electrochemical sensor) can achieve a low LoD as well as have a low cost, but the response time and recovery time are longer than that of the SEIRA spectroscopic waveguide sensor. Also, some functional materials need to be activated at non-room temperature, and the response may get worse over time.[38−40] The main drawback of a refractive index sensor is its poor selectivity, which limits the application of such a technique.[41,42] The proposed SEIRA spectroscopic sensor has the advantages of selectivity and sensitivity.[17] However, high cost may be an obvious shortcoming of an optical sensor, which is expected to be addressed with the maturation of the fabrication technology of infrared laser sources and detectors and the machining technology of optics.

4. CONCLUSIONS

We proposed a SEIRA spectroscopic ChG waveguide sensor based on a Ag island film. The main novelty of this work was the integration of the metal island film with the ChG waveguide sensor to generate a SEIRA effect and to enhance the infrared absorption of the analyte. Compared with other methods for improving the waveguide sensing performance, the metal island film-based SEIRA spectroscopic waveguide sensor can be fabricated with a simple and less time-consuming way. Through C_2H_6O sensing at an NIR wavelength of 1654 nm and the CH_4 sensing at an MIR wavelength of 3291 nm, the ChG waveguide integrated with the Ag island film with a thickness of 1.8 nm shows the best sensing performance among the five fabricated waveguide sensors. In addition to an acceptable α_{int}, the WG3 sensor shows absorbance enhancement factors of >1.5 and >2.3 for C_2H_6O and CH_4, respectively. The 1σ LoD of WG3 is ~4.11% at an averaging time of 0.2 s, and the response time is <0.2 s. Shale gas measurement was performed to validate the normal operation of the sensor. Without changing the structural parameters, the absorption enhancement effect of the SEIRA spectroscopic waveguide using the Ag island film can be realized in both NIR and MIR ranges. Also, the proposed rectangular waveguide sensor with enhanced absorption provides an idea for the design of a sensor-on-a-chip. Future work is to reduce the system noise to further improve the sensing performance.

■ ASSOCIATED CONTENT

ⓈⒾ Supporting Information

The Supporting Information is available free of charge at https://pubs.acs.org/doi/10.1021/acsami.1c08177.

> SEM images of sensors, details of the liquid water-sensing experiment, derivation process of eq 8, and comparison between the SEIRA spectroscopic waveguide gas sensor and other types of waveguide gas sensors (PDF)

■ AUTHOR INFORMATION

Corresponding Author

    Chuantao Zheng − *State Key Laboratory of Integrated Optoelectronics, College of Electronic Science and Engineering, Jilin University, Changchun 130012, China;* ⓘ orcid.org/0000-0001-8008-466X; Email: zhengchuantao@jlu.edu.cn

Authors

    Mingquan Pi − *State Key Laboratory of Integrated Optoelectronics, College of Electronic Science and Engineering, Jilin University, Changchun 130012, China*

    Jialin Ji − *State Key Laboratory of Integrated Optoelectronics, College of Electronic Science and Engineering, Jilin University, Changchun 130012, China*

    Huan Zhao − *State Key Laboratory of Integrated Optoelectronics, College of Electronic Science and Engineering, Jilin University, Changchun 130012, China*

    Zihang Peng − *State Key Laboratory of Integrated Optoelectronics, College of Electronic Science and Engineering, Jilin University, Changchun 130012, China*

    Jiaming Lang − *State Key Laboratory of Integrated Optoelectronics, College of Electronic Science and Engineering, Jilin University, Changchun 130012, China*

    Lei Liang − *State Key Laboratory of Luminescence and Applications, Changchun Institute of Optics Fine Mechanics*

and Physics, Chinese Academy of Sciences, Changchun 130033, China

Yu Zhang − State Key Laboratory of Integrated Optoelectronics, College of Electronic Science and Engineering, Jilin University, Changchun 130012, China; ⓘ orcid.org/ 0000-0003-2100-621X

Yiding Wang − State Key Laboratory of Integrated Optoelectronics, College of Electronic Science and Engineering, Jilin University, Changchun 130012, China

Frank K. Tittel − Department of Electrical and Computer Engineering, Rice University, Houston, Texas 77005, United States

Complete contact information is available at:
https://pubs.acs.org/10.1021/acsami.1c08177

Author Contributions

M.P. fabricated the sensors, performed gas and liquid experiments, performed data analysis, and wrote the manuscript; C.Z. performed data analysis, revised the manuscript, and got funding for the work; J.J. performed sensor simulation and assisted in the gas- and liquid-sensing experiments; H.Z. calibrated the film thickness and assisted in the gas- and liquid-sensing experiments; Z.P. analyzed and verified the sensing results; J.L. fabricated the PDMS gas cell and assisted in the gas- and liquid-sensing experiments; L.L. provided technical guidance and made comments on the manuscript; Y.Z. got funding and made comments on the manuscript; Y.W. got funding and provided technical guidance for the work; and F.K.T. provided technical guidance and revised the manuscript. The manuscript was written through contributions of all authors. All authors have given approval to the final version of the manuscript. Y.W. supported the experiments.

Notes

The authors declare no competing financial interest.

■ REFERENCES

(1) Liu, Z.; Zheng, C.; Zhang, T.; Li, Y.; Ren, Q.; Chen, C.; Ye, W.; Zhang, Y.; Wang, Y.; Tittel, F. K. Midinfrared Sensor System Based on Tunable Laser Absorption Spectroscopy for Dissolved Carbon Dioxide Analysis in the South China Sea: System-Level Integration and Deployment. *Anal. Chem.* **2020**, *92*, 8178−8185.

(2) Zheng, K.; Zheng, C.; Li, J.; Ma, N.; Liu, Z.; Li, Y.; Zhang, Y.; Wang, Y.; Tittel, F. K. Novel Gas-Phase Sensing Scheme Using Fiber-Coupled Off-Axis Integrated Cavity Output Spectroscopy (FC-OA-ICOS) and Cavity-Reflected Wavelength Modulation Spectroscopy (CR-WMS). *Talanta* **2020**, *213*, 120841.

(3) Zheng, K.; Zheng, C.; Li, J.; Ma, N.; Liu, Z.; Zhang, Y.; Wang, Y.; Tittel, F. K. Near-Infrared Methane Sensor System Using Off-Axis Integrated Cavity Output Spectroscopy with Novel Dual-Input Dual-Output Coupling Scheme for Mode Noise Suppression. *Sens. Actuators, B* **2020**, *308*, 127674.

(4) Zheng, K.; Zheng, C.; Ma, N.; Liu, Z.; Yang, Y.; Zhang, Y.; Wang, Y.; Tittel, F. K. Near-Infrared Broadband Cavity-Enhanced Spectroscopic Multigas Sensor Using a 1650 nm Light Emitting Diode. *ACS Sens.* **2019**, *4*, 1899−1908.

(5) Hu, L.; Zheng, C.; Zhang, M.; Yao, D.; Zheng, J.; Zhang, Y.; Wang, Y.; Tittel, F. K. Quartz-Enhanced Photoacoustic Spectroscopic Methane Sensor System Using a Quartz Tuning Fork-Embedded, Double-Pass and Off-Beam Configuration. *Photoacoustics* **2020**, *18*, 100174.

(6) Schwarz, B.; Reininger, P.; Ristanić, D.; Detz, H.; Andrews, A. M.; Schrenk, W.; Strasser, G. Monolithically Integrated Mid-Infrared Lab-On-a-Chip Using Plasmonics and Quantum Cascade Structures. *Nat. Commun.* **2014**, *5*, 4085.

(7) Kumari, B.; Barh, A.; Varshney, R. K.; Pal, B. P. Silicon-on-Nitride Slot Waveguide: A Promising Platform as Mid-IR Trace Gas Sensor. *Sens. Actuators, B* **2016**, *236*, 759−764.

(8) Kumari, B.; Varshney, R. K.; Pal, B. P. Design of Chip Scale Silicon Rib Slot Waveguide for Sub-Ppm Detection of N_2O Gas at Mid-IR Band. *Sens. Actuators, B* **2018**, *255*, 3409−3416.

(9) Siebert, R.; Müller, J. Infrared Integrated Optical Evanescent Field Sensor for Gas Analysis Part I: System Design. *Sens. Actuators, A* **2005**, *119*, 138−149.

(10) Siebert, R.; Müller, J. Infrared Integrated Optical Evanescent Field Sensor for Gas Analysis Part II. Fabrication. *Sens. Actuators, A* **2005**, *119*, 584−592.

(11) Lavchiev, V. M.; Jakoby, B. Photonics in the Mid-Infrared: Challenges in Single-Chip Integration and Absorption Sensing. *IEEE J. Sel. Top. Quant. Electron.* **2017**, *23*, 8200612.

(12) Gutierrez-Arroyo, A.; Baudet, E.; Bodiou, L.; Lemaitre, J.; Hardy, I.; Faijan, F.; Bureau, B.; Nazabal, V.; Charrier, J. Optical Characterization at 7.7 μm of an Integrated Platform Based on Chalcogenide Waveguides for Sensing Applications in the Mid-Infrared. *Opt. Express* **2016**, *24*, 23109−23117.

(13) Huang, Y.; Kalyoncu, S. K.; Zhao, Q.; Torun, R.; Boyraz, O. Silicon-on-Sapphire Waveguides Design for Mid-IR Evanescent Field Absorption Gas Sensors. *Opt. Commun.* **2014**, *313*, 186−194.

(14) Dell'Olio, F.; Passaro, V. M. Optical Sensing by Optimized Silicon Slot Waveguides. *Opt. Express* **2007**, *15*, 4977−4993.

(15) Kita, D. M.; Michon, J.; Johnson, S. G.; Hu, J. Are Slot and Sub-Wavelength Grating Waveguides Better than Strip Waveguides for Sensing? *Optica* **2018**, *5*, 1046−1054.

(16) Pi, M.; Zheng, C.; Bi, R.; Zhao, H.; Liang, L.; Zhang, Y.; Wang, Y.; Tittel, F. K. Design of a Mid-Infrared Suspended Chalcogenide/Silica-on-Silicon Slot-Waveguide Spectroscopic Gas Sensor with Enhanced Light-Gas Interaction Effect. *Sens. Actuators, B* **2019**, *297*, 126732.

(17) Pi, M.; Zheng, C.; Peng, Z.; Zhao, H.; Lang, J.; Liang, L.; Zhang, Y.; Wang, Y.; Tittel, F. K. Theoretical Study of Microcavity-Enhanced Absorption Spectroscopy for Mid-Infrared Methane Detection Using a Chalcogenide/Silica-on-Fluoride Horizontal Slot-Waveguide Racetrack Resonator. *Opt. Express* **2020**, *28*, 21432−21446.

(18) Tombez, L.; Zhang, E. J.; Orcutt, J. S.; Kamlapurkar, S.; Green, W. M. J. Methane Absorption Spectroscopy on a Silicon Photonic Chip. *Optica* **2017**, *4*, 1322−1325.

(19) Han, Z.; Lin, P.; Singh, V.; Kimerling, L.; Hu, J.; Richardson, K.; Agarwal, A.; Tan, D. T. H. On-Chip Mid-Infrared Gas Detection Using Chalcogenide Glass Waveguide. *Appl. Phys. Lett.* **2016**, *108*, 141106.

(20) Lai, W.-C.; Chakravarty, S.; Wang, X.; Lin, C.; Chen, R. T. On-Chip Methane Sensing by Near-IR Absorption Signatures in a Photonic Crystal Slot Waveguide. *Opt. Lett.* **2011**, *36*, 984−986.

(21) Lai, W.-C.; Chakravarty, S.; Wang, X.; Lin, C.; Chen, R. T. Photonic Crystal Slot Waveguide Absorption Spectrometer for On-Chip Near-Infrared Spectroscopy of Xylene in Water. *Appl. Phys. Lett.* **2011**, *98*, 023304.

(22) Gervais, A.; Jean, P.; Shi, W.; LaRochelle, S. Design of Slow-Light Subwavelength Grating Waveguides for Enhanced On-Chip Methane Sensing by Absorption Spectroscopy. *IEEE J. Sel. Top. Quant. Electron.* **2019**, *25*, 5200308.

(23) Yoo, K. M.; Midkiff, J.; Rostamian, A.; Chung, C.-j.; Dalir, H.; Chen, R. T. InGaAs Membrane Waveguide: A Promising Platform for

Monolithic Integrated Mid-Infrared Optical Gas Sensor. *ACS Sens.* **2020**, *5*, 861−869.

(24) Stievater, T. H.; Pruessner, M. W.; Park, D.; Rabinovich, W. S.; Andrew McGill, R.; Kozak, D. A.; Furstenberg, R.; Holmstrom, S. A.; Khurgin, J. B. Trace Gas Absorption Spectroscopy Using Functionalized Microring Resonators. *Opt. Lett.* **2014**, *39*, 969−972.

(25) Chen, C.; Mohr, D. A.; Choi, H.-K.; Yoo, D.; Li, M.; Oh, S.-H. Waveguide-Integrated Compact Plasmonic Resonators for On-Chip Mid-Infrared Laser Spectroscopy. *Nano Lett.* **2018**, *18*, 7601−7608.

(26) Mohr, D. A.; Yoo, D.; Chen, C.; Li, M.; Oh, S.-H. Waveguide-Integrated Mid-Infrared Plasmonics with High-Efficiency Coupling for Ultracompact Surface-Enhanced Infrared Absorption Spectroscopy. *Opt. Express* **2018**, *26*, 23540−23549.

(27) Chen, C.; Oh, S.-H.; Li, M. Coupled-Mode Theory for Plasmonic Resonators Integrated with Silicon Waveguides towards Mid-Infrared Spectroscopic Sensing. *Opt. Express* **2020**, *28*, 2020−2036.

(28) Cheruvalath, A.; Nampoori, V. P. N.; Thomas, S. Oblique Angle Deposited Silver Islands on $Ge_{20}Se_{70}Te_{10}$ Film Substrate for Surface-Enhanced Infrared Spectroscopy. *Sens. Actuators, B* **2019**, *287*, 225−230.

(29) Hartstein, A.; Kirtley, J.; Tsang, J. Enhancement of the Infrared Absorption from Molecular Monolayers with Thin Metal Overlayers. *Phys. Rev. Lett.* **1980**, *45*, 201204.

(30) https://refractiveindex.info/ (accessed January 20, 2021).

(31) Vlk, M.; Datta, A.; Alberti, S.; Yallew, H. D.; Mittal, V.; Murugan, G. S.; Jágerská, J. Extraordinary Evanescent Field Confinement Waveguide Sensor for Mid-infrared Trace Gas Spectroscopy. *Light: Sci. Appl.* **2021**, *10*, 26.

(32) Zhao, Y.; Li, C.; Guo, P.; Zhang, W.; Xu, P.; Zhang, P. Exploration of Lift-Off Ge−As−Se Chalcogenide Waveguides with Thermal Reflow Process. *Opt. Mater.* **2019**, *92*, 206−211.

(33) Nakashima, H.; Sasaki, Y.; Osozawa, R.; Kon, Y.; Nakazawa, H.; Suzuki, Y. Surface Enhanced Infrared Absorption Spectra on Pulsed Laser Deposited Silver Island Films. *Thin Solid Films* **2013**, *536*, 166−171.

(34) Osawa, M.; Ikeda, M. Surface-Enhanced Infrared Absorption of P-Nitrobenzoic Acid Deposited on Silver Island films: Contributions of Electromagnetic and Chemical Mechanisms. *J. Phys. Chem.* **1991**, *95*, 9914−9919.

(35) Li, C.; Zheng, C.; Dong, L.; Ye, W.; Tittel, F. K.; Wang, Y. Ppb-Level Mid-Infrared Ethane Detection Based on Three Measurement Schemes Using a 3.34-μm Continuous-Wave Interband Cascade Laser. *Appl. Phys. B* **2016**, *122*, 185.

(36) Li, S.; Meng, F.; Zhang, X.; Zhou, Z.; Shen, B.; Wei, S.; Zhang, S. Gas Composition and Carbon Isotopic Variation During Shale Gas Desorption: Implication from the Ordovician Wufeng Formation - Silurian Longmaxi Formation in West Hubei, China. *J. Nat. Gas Sci. Eng.* **2021**, *87*, 103777.

(37) Su, P.; Han, Z.; Kita, D.; Becla, P.; Lin, H.; Deckoff-Jones, S.; Richardson, K.; Kimerling, L. C.; Hu, J.; Agarwal, A. Monolithic On-Chip Mid-IR Methane Gas Sensor with Waveguide-Integrated Detector. *Appl. Phys. Lett.* **2019**, *114*, 051103.

(38) Gao, H.; Yu, Q.; Chen, K.; Sun, P.; Liu, F.; Yan, X.; Liu, F.; Lu, G. Ultrasensitive Gas Sensor Based on Hollow Tungsten Trioxide-Nickel Oxide (WO_3-NiO) Nanoflowers for Fast and Selective Xylene Detection. *J. Colloid Interface Sci.* **2019**, *535*, 458−468.

(39) He, J.; Yan, X.; Liu, A.; You, R.; Liu, F.; Li, S.; Wang, J.; Wang, C.; Sun, P.; Yan, X.; Kang, B.; He, J.; Wang, Y.; Lu, G. A Rapid-Response Room-Temperature Planar Type Gas Sensor Based on DPA-Ph-DBPzDCN for the Sensitive Detection of NH_3. *J. Mater. Chem. A* **2019**, *7*, 4744.

(40) Chen, R.; Wang, J.; Luo, S.; Xiang, L.; Li, W.; Xie, D. Unraveling Photoexcited Electron Transfer Pathway of Oxygen Vacancy-Enriched ZnO/Pd Hybrid toward Visible Light-Enhanced Methane Detection at a Relatively Low Temperature. *Appl. Catal., B* **2020**, *264*, 118554.

(41) Zhang, Y.; Zou, J.; Cao, Z.; HE, J.-J. Temperature-Insensitive Waveguide Sensor Using a Ring Cascaded with a Mach−Zehnder Interferometer. *Opt. Lett.* **2019**, *44*, 299−302.

(42) Smith, C. J.; Shankar, R.; Laderer, M.; Frish, M. B.; Loncar, M.; Allen, M. G. Sensing Nitrous Oxide with QCL-Coupled Silicon-on-Sapphire Ring Resonators. *Opt. Express* **2015**, *23*, 5491−5499.